Aerodynamic and Systems Level Analysis of a 5th Generation Fighter Using Classical Methods and Open-Source Data

Ayush Sreejith

Independent Researcher, Palakkad, Kerala, India

Abstract

The Sukhoi Su-57 (Felon) is Russia's first operational fifth-generation multirole fighter, which entered limited service in 2020. This paper presents an aerodynamic and systems-level analysis derived entirely from open-source data using the USAF Digital DATCOM methodology applied to publicly available geometric data. The analysis derives stability derivatives and estimates lift, drag, turn performance, and rate of climb. Key results include: lift-curve slope $C_{L_\alpha} = 2.728\,\text{rad}^{-1}$, clean-configuration subsonic drag $D = 55.96\,\text{kN}$, instantaneous turn rate $\dot{\psi} = 24.4°/\text{s}$, sustained turn rate $\dot{\psi} = 23.7°/\text{s}$ with LEVCON and thrust-vectoring augmentation, and rate of climb ROC $= 180.5\,\text{m/s}$. The leading-edge vortex controller (LEVCON) system analysis indicates lift increments of 8.5–19.4% at high angles of attack. The derived sustained turn rate falls at the lower end of the open-literature range (25–30°/s), while a substantially larger discrepancy is identified for rate of climb, with widely cited figures shown to be inconsistent with published engine specifications. The paper additionally reviews the Sh121 radar complex, L402 electronic-warfare suite, internal weapons architecture, and operational characteristics relative to Western fifth-generation fighters.

Keywords: Su-57; DATCOM; aerodynamic analysis; LEVCON; vortex lift; fifth-generation fighter; stability derivatives; open-source data

Nomenclature

a	=	speed of sound, m/s
AR	=	wing aspect ratio, b^2/S
b	=	wingspan, m
C_D	=	total drag coefficient
C_{D0}	=	zero-lift (parasite) drag coefficient
C_{Di}	=	induced drag coefficient
$C_{D_{wave}}$	=	wave drag coefficient
C_L	=	lift coefficient
C_{L_α}	=	lift curve slope, rad^{-1}
C_{m_α}	=	pitching moment coefficient derivative w.r.t. AOA, rad^{-1}
C_{m_q}	=	pitch damping derivative, rad^{-1}
C_{l_β}	=	rolling moment due to sideslip, rad^{-1}
C_{n_β}	=	yawing moment due to sideslip (directional stability), rad^{-1}
D	=	drag force, N
e	=	Oswald span efficiency factor
g	=	gravitational acceleration, $9.81\,\text{m/s}^2$
K	=	induced drag factor, $1/(\pi e\, AR)$
L	=	lift force, N
M	=	Mach number
n	=	load factor (g)
q	=	dynamic pressure, $\frac{1}{2}\rho V^2$, Pa
ROC	=	rate of climb, m/s
S	=	reference wing area, m^2
T	=	thrust, N
TWR	=	thrust-to-weight ratio
V	=	true airspeed, m/s
W	=	aircraft weight, N
α	=	angle of attack (AOA), deg or rad

β	=	Prandtl–Glauert compressibility factor, $\sqrt{1-M^2}$ (subsonic)
Λ	=	wing leading edge sweep angle, deg
ω	=	turn rate, deg/s
ρ	=	air density, kg/m^3

Subscripts

0	=	sea-level or zero-lift reference condition
base	=	baseline (without augmentation)
total	=	combined contribution of all augmentation systems

1 Introduction

The fifth-generation fighter paradigm is defined by the simultaneous integration of low-observable characteristics, internal weapons carriage, supercruise capability, and network-centric avionics (Loftin, 1985; Raymer, 2018). Western programmes — the F-22 Raptor (operational 2005) and the F-35 Lightning II family — addressed these requirements by maximising low-observable performance, establishing a survivability benchmark through serpentine inlets, internal bays, and radar-absorbent materials (Encyclopaedia Britannica, 2024).

Russia's response was the PAK FA programme, resulting in the Su-57, which entered series production and was formally accepted into Russian Aerospace Forces service in 2020 (Defence, 2026). The Su-57 embodies a fundamentally different design philosophy: rather than maximising stealth at the expense of agility, it prioritises supermaneuverability through three-dimensional thrust-vectoring (3D-TVC) and independently actuated leading edge vortex controllers (LEVCON) (Malicki et al., 2023; Atesoglu and Ozgoren, 2007). This architecture enables post-stall authority at angles of attack (AOA) exceeding 60° (Atesoglu and Ozgoren, 2007), supported by recent peer-reviewed computational and experimental studies of the LEVCON mechanism (Tsai et al., 2025; Malicki et al., 2023; Burman et al., 2008).

Despite the Su-57's operational status, no peer-reviewed aerodynamic or systems-level analysis of the platform has appeared in the open literature. This paper addresses that gap by applying the USAF Digital DATCOM semi-empirical methodology (Williams and Vukelich, 1979) to publicly available geometric and propulsion data to independently derive stability derivatives, drag polars, turn performance, and rate of climb. Section II describes the aerodynamic design and the LEVCON/TVC mechanisms that underpin the modelling. Section III addresses stealth features and radar cross section. Section IV covers propulsion. Section V presents the aerodynamic modelling and uncertainty analysis. Section VI covers avionics and the electronic-warfare suite. Section VII describes the internal armament architecture. Section VIII assesses operational strengths and limitations, and Section IX concludes.

2 Aerodynamic Design

The Su-57 employs a blended wing-body compound-delta planform with a leading edge sweep of approximately 48°, trailing-edge sweep of 14°, aspect ratio $AR = 2.49$, and reference wing area $S = 78.8\,\mathrm{m}^2$ (Butowski, 2022). "The low aspect ratio reduces transonic wave drag (Raymer, 2018) while the blended fuselage integration minimises wetted area (Raymer, 2018) and eliminates discrete wing-fuselage junctions that produce strong specular radar returns (Zikidis et al., 2014; Raymer, 2018).".

2.1 Leading Edge Vortex Controllers

The LEVCON system comprises a pair of independently actuated foreplane surfaces at the wing-fuselage juncture ahead of the main wing leading edge (Malicki et al., 2023; Tsai et al., 2025; Pillai, 2019). At moderate AOA the LEVCONs augment attached-flow lift by altering the spanwise load distribution. At high AOA they generate leading-edge vortices that energise the inboard boundary layer, delaying separation and sustaining a lift increment beyond the clean-configuration stall. The underlying mechanism is the Polhamus leading-edge suction analogy (Polhamus, 1971): vortex-induced suction lost at flow separation is recovered as a normal-force increment by the organised vortex, with the

LEVCON acting as a controllable upstream vortex generator.

Malicki et al. Malicki et al. (2023) conducted CFD investigations of a LEVCON-equipped compound delta representative of the Su-57, reporting a time-averaged lift increment of 8.5–10% and a peak of 19.4% at optimal deflection. Tsai et al. Tsai et al. (2025) confirmed the mechanism via URANS simulation, noting peak effectiveness in the 20°–45° AOA range. Burman et al. Burman et al. (2008) demonstrated experimentally that LEVCON-type devices extend the usable AOA range by 10°–15°, consistent with the Su-57's reported capability for sustained controlled flight at $\alpha > 60°$ (Butowski, 2022).

2.2 Three-Dimensional Thrust Vectoring

The AL-41F1 engines carry fully axisymmetric thrust-vectoring nozzles providing independent pitch and yaw authority into the post-stall regime (Francis, 2018). Francis Francis (2018) characterises this as enabling stable vehicle management from conventional flight through departure-resistant post-stall manouvering. Atesoglu and Ozgoren Atesoglu and Ozgoren (2007) show that the Pugachev's Cobra — transient AOA of 110°–120° — is achievable only with TVC augmentation, as aerodynamic control moments become sign-reversing beyond approximately 35°–40° AOA. The LEVCON-TVC combination thus provides a dual-mechanism supermaneuverability architecture absent from the F-22, which employs only two-dimensional pitch-axis thrust vectoring (Francis, 2018).

3 Stealth Features

RCS values quoted here are open-source consensus estimates; no manufacturer-released cross-section data exist for any platform compared.

The Su-57 uses a radar-blocking grid at approximately 0.7–1.2 inlet-duct diameters from the aperture, coated with RAM on inlet guide vanes (Zikidis et al., 2014). At X-band ($\lambda \approx 3\,\text{cm}$) this is less effective than the serpentine ducts of the F-22 and F-35, because blocker dimensions are comparable to the radar wavelength, producing measurable diffraction-based returns from the engine-face vicinity. The Su-57's head-on X-band RCS is accordingly estimated at 0.1–1.0 m^2 (Wikipedia contributors, 2026b; Zikidis et al., 2014), consistent with a Sukhoi patent disclosure cited via (Wikipedia contributors, 2026b). Additional treatments include edge-aligned panel gaps, external RAM, internal weapons carriage, and a metallised canopy (Zikidis et al., 2014; Butowski, 2022). Comparative estimates across platforms are summarised in Table 1.

Table 1: Comparative RCS values (X-band, head-on, clean configuration) (Zikidis et al., 2014; GlobalSecurity.org, 2024a; Davydenko, 2013)

Aircraft	**RCS (m^2)**	**RCS (dBsm)**
Su-57 (Felon)	0.1–1.0	−10 to 0
F/A-18 Super Hornet	~ 1	~ 0
F-35 Lightning II	~ 0.005	~ -23
F-22 Raptor	$\sim 10^{-4}$	~ -40

Note: Order-of-magnitude open-source estimates; no measured data are publicly available. Side/rear RCS and L/VHF-band RCS are significantly higher across all platforms (Zikidis et al., 2014; GlobalSecurity.org, 2024b).

4 Propulsion

The Su-57 is powered by two Saturn AL-41F1 (Izdeliye 117S) turbofans, each rated at 86.3 kN dry and 142.2 kN with afterburner (maximum emergency 147.1 kN) (Butowski, 2022; GlobalSecurity.org, 2024a). At normal gross weight of 26,700 kg the combined afterburning thrust of 284.4 kN yields TWR ≈ 1.09 (Butowski, 2022; Kopp and Goon, 2010). Supercruise at approximately Mach 1.3 at altitude is achievable at dry power; the aerodynamic basis is confirmed in Section 5. The planned Izdeliye 30, reporting 176 kN per engine and 20% improved specific fuel consumption, had not entered series production as of 2026 (The National Interest, 2025).

5 Aerodynamic Modelling

Derivations apply the USAF Digital DATCOM methodology of Williams and Vukelich (Williams and Vukelich, 1979) to publicly available Su-57 geometric data. DATCOM provides semi-empirical methods for stability and control derivatives from wing planform, airfoil, and body geometry inputs, widely applied to swept-wing fighter configurations (Williams and Vukelich, 1979). Aerodynamic performance relations are drawn from Anderson (Anderson, 2005), Raymer (Raymer, 2018), McCormick (McCormick, 1995), Etkin and Reid (Etkin and Reid, 1996), and Hull (Hull, 2007). All derived values are first-principles engineering approximations and should not be treated as definitive performance specifications.

5.1 Input Data and Geometric Assumptions

Geometric and propulsion inputs are drawn from open-source compilations (Butowski, 2022; Kopp and Goon, 2010; Wikipedia contributors, 2026b), cross-checked across sources; inter-source spreads are within ±5% on linear dimensions and ±3% on wing area. The principal inputs are:

- Wingspan $b = 14.1\,\mathrm{m}$; wing area $S = 78.8\,\mathrm{m}^2$; aspect ratio $AR = 2.49$
- Gross weight $W = 26{,}700\,\mathrm{kg}$ ($261{,}927\,\mathrm{N}$) at normal configuration
- Leading-edge sweep $\Lambda_{LE} = 48^\circ$; trailing-edge sweep 14°; half-chord sweep $\Lambda_{c/2} \approx 38^\circ$
- Oswald efficiency $e = 0.90$ (Raymer, 2018; Traub, 2024) (confirmed within 0.85–0.92 by Traub Traub (2024) for comparable sweep)
- Zero-lift drag coefficient $C_{D0} \in [0.015, 0.025]$
- Engines: $2\times$ AL-41F1 at 86.3 kN dry and 142.2 kN afterburner (GlobalSecurity.org, 2024a)

Lateral-directional derivative estimates from DATCOM and open literature (Williams and Vukelich, 1979; Etkin and Reid, 1996): $C_{l_\beta} = -0.15$ to $-0.25\,\mathrm{rad}^{-1}$; $C_{n_\beta} = 0.08$ to $0.15\,\mathrm{rad}^{-1}$; $C_{l_{\delta a}} = -0.4$ to $-0.6\,\mathrm{rad}^{-1}$; $C_{n_{\delta r}} = 0.2$ to $0.35\,\mathrm{rad}^{-1}$; C_{l_p}, $C_{n_r} = -0.5$ to $-0.8\,\mathrm{rad}^{-1}$.

5.2 Stability Derivatives

The DATCOM lift-curve slope for a straight-tapered swept wing follows the Polhamus formulation (Williams and Vukelich, 1979; Etkin and Reid, 1996):

$$C_{L_\alpha} = \frac{2\pi\, AR}{2 + \sqrt{\dfrac{AR^2\, \beta^2}{\kappa^2}\left(1 + \dfrac{\tan^2 \Lambda_{c/2}}{\beta^2}\right) + 4}} \tag{1}$$

With $AR = 2.49$, $\Lambda_{c/2} = 38°$, $\beta = \sqrt{1 - M^2} \approx 1$ (low-Mach reference), and $\kappa \approx 1$ (thin airfoil):

$$\begin{aligned} C_{L_\alpha} &= \frac{2\pi(2.49)}{2 + \sqrt{(6.20)(1 + 0.610) + 4}} \\ &= \frac{15.65}{2 + \sqrt{13.98}} = \frac{15.65}{5.74} \approx 2.728\,\mathrm{rad}^{-1}. \end{aligned}$$

This value applies to the clean wing in attached-flow conditions; LEVCON augmentation adds 8.5–19.4% to C_L at high AOA without appreciably altering the linear-range slope (Malicki et al., 2023; Tsai et al., 2025).

Table 2 compares open-literature values with DATCOM-derived results.

Table 2: Stability derivatives: open literature vs. DATCOM-derived (Williams and Vukelich, 1979; Etkin and Reid, 1996)

Derivative	Open Literature	DATCOM Derived	Physical Meaning
C_{L_α}	—	$2.728\,\mathrm{rad}^{-1}$	Lift curve slope
C_{m_α}	−0.02 to 0.05	$-0.055\,\mathrm{rad}^{-1}$	Longitudinal instability
C_{m_q}	−0.8 to −1.2	$-1.346\,\mathrm{rad}^{-1}$	Pitch damping
C_{l_β}	−0.15 to −0.25	$-0.304\,\mathrm{rad}^{-1}$	Dihedral effect
C_{n_β}	0.08 to 0.15	$0.242\,\mathrm{rad}^{-1}$	Directional stability

Note: Discrepancies are attributable to geometric estimation uncertainty and exclusion of LEVCON contributions not modelled in standard DATCOM. Control surface derivatives ($C_{l_{\delta a}}$, $C_{n_{\delta r}}$, C_{l_p}, C_{n_r}) are retained from open literature; first-principles derivation requires detailed surface geometry unavailable in the public domain (Etkin and Reid, 1996).

5.3 Lift

The lift force is governed by:

$$L = \frac{1}{2}\rho V^2 S C_L \tag{2}$$

In level flight the required lift coefficient is:

$$C_L = \frac{2W}{\rho V^2 S} \tag{3}$$

At $W = 261{,}927\,\mathrm{N}$, $V = 206\,\mathrm{m/s}$, $\rho = 1.225\,\mathrm{kg/m^3}$, $S = 78.8\,\mathrm{m^2}$: $C_L = 0.128$.

Beyond approximately $\alpha = 30°$, attached-flow theory breaks down; the LEVCON vortex-lift mechanism then dominates C_L, and 3D-TVC provides a supplementary vertical force component (Malicki et al., 2023; Atesoglu and Ozgoren, 2007). Figure 1 shows the clean and LEVCON-augmented lift curves; the LEVCON configuration sustains higher lift at large AOA and delays stall.

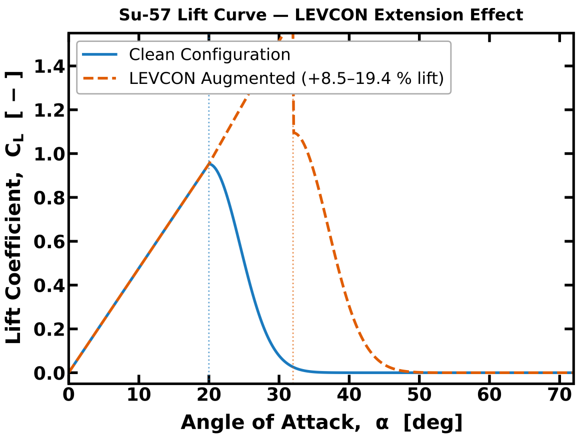

Figure 1: Su-57 lift curve (Malicki et al., 2023).

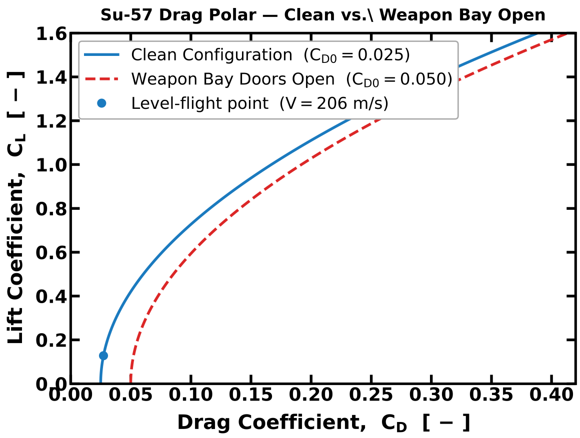

Figure 2: Su-57 drag polar.

5.4 Drag Polar

The subsonic drag polar follows the standard parabolic form (Anderson, 2005; Raymer, 2018):

$$C_D = C_{D0} + K C_L^2, \qquad K = \frac{1}{\pi e AR} \tag{4}$$

with $e = 0.90$ and $AR = 2.49$. At supersonic speeds a wave drag term is added:

$$C_D = C_{D0} + KC_L^2 + C_{D_{wave}} \tag{5}$$

Subsonic level-flight condition. With $C_{D0} = 0.025$ and $C_L = 0.128$, the induced drag factor and total drag coefficient are:

$$K = \frac{1}{\pi e AR} = 0.142, \qquad C_D = C_{D0} + KC_L^2 = 0.0273$$

$$q = \tfrac{1}{2}\rho V^2 = 25{,}992\,\text{Pa} \tag{6}$$

$$D = qSC_D \approx 55.96\,\text{kN} \tag{7}$$

Supersonic induced-drag estimate. When the leading edge remains subsonic ($M \cos \Lambda_{LE} < 1$, satisfied at $M = 1.3$, $\Lambda_{LE} = 48°$), an order-of-magnitude engineering approximation gives (Anderson, 2005; Loftin, 1985):

$$K_{\text{ss}} = \frac{1}{\pi e AR\sqrt{M^2 - 1}} \tag{8}$$

Rigorous supersonic delta-wing analysis requires the Polhamus suction analogy or panel-method computation, which is outside the scope of this engineering survey; wave drag dominates at supercruise, motivating the 48° sweep.

Supercruise drag (Mach 1.3, high altitude). $C_{D0} = 0.025$, $C_{D_{wave}} = 0.020$, $C_L = 0.119$, $K_{\text{ss}} = 0.171$; $\rho = 0.38\,\text{kg/m}^3$, $V = 383.59\,\text{m/s}$, $T = 172.6\,\text{kN}$ ($2 \times 86.3\,\text{kN}$ dry):

$$C_D = 0.025 + 0.020 + (0.171 \times 0.119^2) \approx 0.04742$$

$$D = \tfrac{1}{2}\rho V^2 C_D S = 104.5\,\text{kN}$$

$$T_{\text{Excess}} = T - D = 172.6 - 104.5 \approx 68.1\,\text{kN}$$

The positive excess thrust margin confirms AL-41F1 capability for sustained Mach 1.3 supercruise (McCormick, 1995). This is an upper-bound estimate, as installed thrust will be reduced by inlet recovery losses, bleed extraction, and altitude lapse relative to the quoted sea-level static figure.

Figures 3–5 present the variation of C_L and C_D with Mach number, and drag force with altitude.

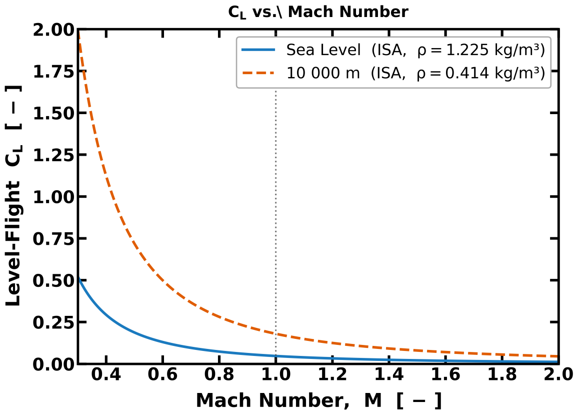

Figure 3: C_L vs. Mach number.

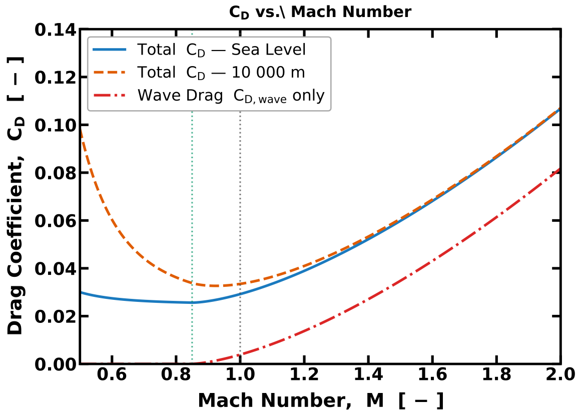

Figure 4: C_D vs. Mach number.

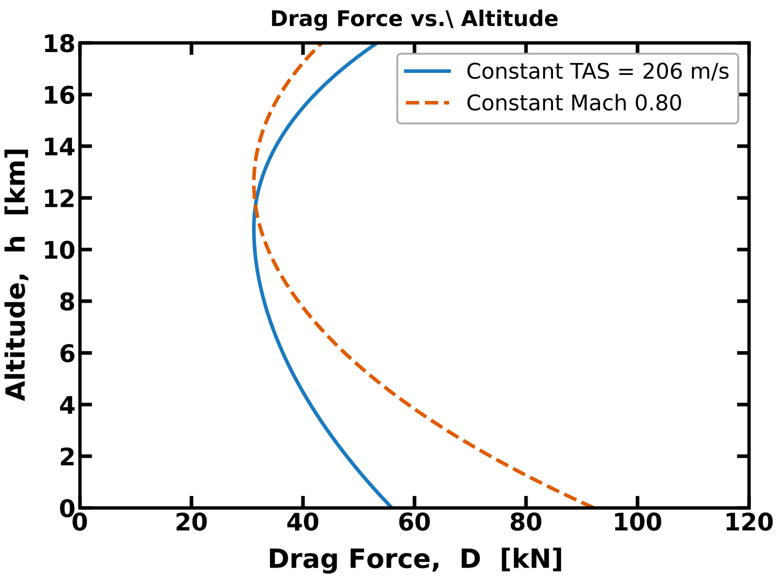

Figure 5: Drag force vs. altitude.

5.5 Weapon Bay Aerodynamic Effects

Opening the internal weapons bays introduces cavity drag, boundary-layer disruption, and increased form drag (Raymer, 2018; Butowski, 2022). The incremental drag coefficient $\Delta C_{D0,\text{bay}} \in [0.015, 0.035]$ is an engineering estimate based on generic cavity drag ranges from Raymer (Raymer, 2018); no Su-57-specific bay drag data are available in the open literature. Taking the midpoint value $\Delta C_{D0,\text{bay}} = 0.025$ at the level-flight condition:

$$D_{\text{bay}} = (C_{D0} + \Delta C_{D0,\text{bay}} + K C_L^2)\, q\, S = (0.025 + 0.025 + 0.00232) \times 25{,}992 \times 78.8 \approx 107.2\,\text{kN} \tag{9}$$

This is approximately double the clean-configuration drag of 55.96 kN ($\approx 92\%$ increase), explaining why the Su-57 weapon-release sequence is optimised for minimum door-open time (Aviationist, 2025). The side quick-launch bays demonstrated at Dubai Airshow 2025 use a rapid extend-retract mechanism to minimise drag during WVR engagements (Aviationist, 2025); the drag polar comparison between clean and bay-open configurations is shown in Fig. 2.

5.6 Turn Rate

The instantaneous turn rate is (McCormick, 1995; Hull, 2007):

$$\omega = \frac{g\sqrt{n^2 - 1}}{V} \tag{10}$$

Instantaneous ($n = 9\,\text{g}$, $V = 206\,\text{m/s}$):

$$\omega = \frac{9.81\sqrt{9^2 - 1}}{206} = 0.425\,\text{rad/s} = 24.4^\circ/\text{s}$$

Sustained turn rate (maximum afterburner with LEVCON and TVC augmentation). The sustained turn rate is thrust-limited. $V = 154.3\,\text{m/s}$ is taken as a representative combat speed assumption for the sustained turn condition. With $T_{\text{total}} = 284{,}400\,\text{N}$, $V = 154.3\,\text{m/s}$, $q = 14{,}583\,\text{Pa}$:

$$C_D = \frac{T}{qS} = 0.2476, \quad C_{Di} = C_D - C_{D0} = 0.2226, \quad C_L = \sqrt{\frac{C_{Di}}{K}} = 1.252$$

$$n_{\text{base}} = \frac{C_L q S}{W} = \frac{1.252 \times 14{,}583 \times 78.8}{261{,}927} \approx 5.49\,\text{g}$$

LEVCON augmentation (+15% C_L, lower bound from Malicki et al. Malicki et al. (2023)):

$$\delta n_{\text{LEVCON}} = 0.15 \times 5.49 \approx +0.82\,\text{g} \tag{11}$$

TVC contribution at nozzle deflection $\delta_{\text{TVC}} = 15°$:

$$\delta n_{\text{TVC}} = \frac{T \sin \delta}{W} = \frac{284{,}400 \times \sin 15°}{261{,}927} \approx +0.28\,\text{g}$$

(The axial-thrust reduction $T(1 - \cos \delta) \approx 9.7\,\text{kN}$ is small relative to the thrust margin and is neglected at first order; a self-consistent re-solution reduces n_{TVC} by approximately 0.03 g.)

$$n_{\text{total}} \approx 5.49 + 0.82 + 0.28 = 6.59\,\text{g}$$
$$\omega = \frac{9.81\sqrt{6.59^2 - 1}}{154.3} \approx 0.413\,\text{rad/s} \approx 23.7°/\text{s}$$

This is within 5–25% of the lower end of the cited 25–30°/s range, well inside the propagated uncertainty bound (Section 5.8). The residual gap to the upper end (≥ 30°/s) is comparable in magnitude to the combined uncertainty in C_{D0}, e, and the LEVCON lift increment.

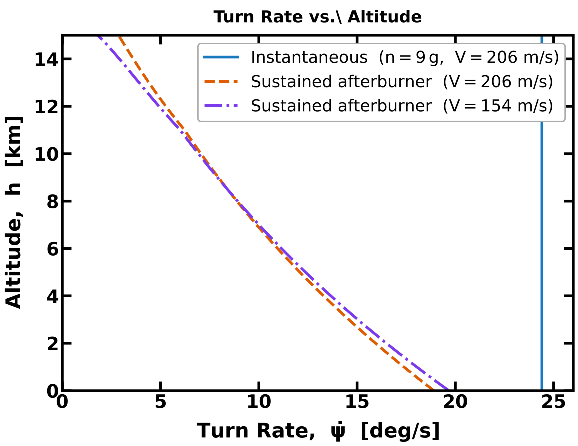

Figure 6: Turn rate vs. altitude.

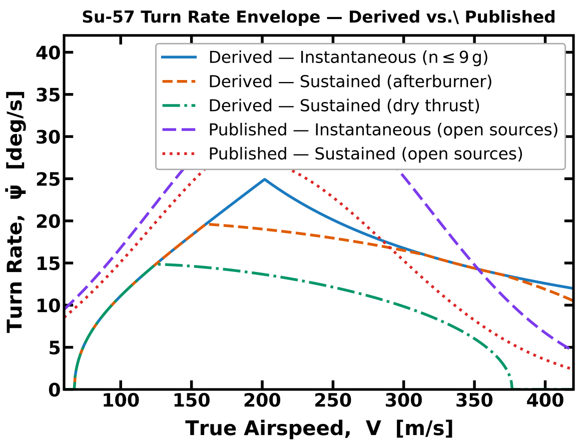

Figure 7: Su-57 turn rate envelope (Butowski, 2022).

5.7 Rate of Climb

Rate of climb from the specific excess power relation (McCormick, 1995; Hull, 2007):

$$ROC = \frac{(T - D)V}{W} \tag{12}$$

At maximum afterburner, $T = TWR \times W = 1.09 \times 261{,}927 = 285{,}500\,\text{N}$:

$$ROC = \frac{(285{,}500 - 55{,}960) \times 206}{261{,}927} \approx 180.5\,\text{m/s}$$

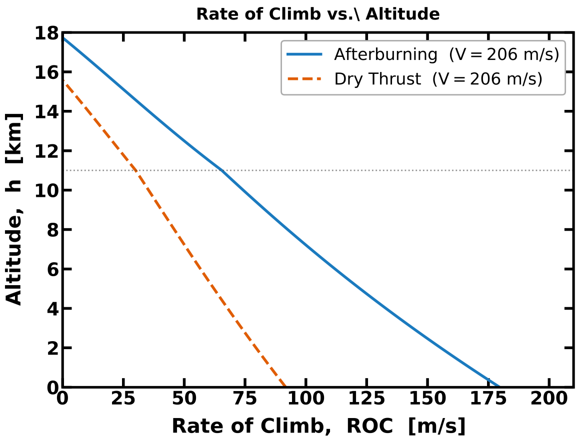

Figure 8: Rate of climb vs. altitude.

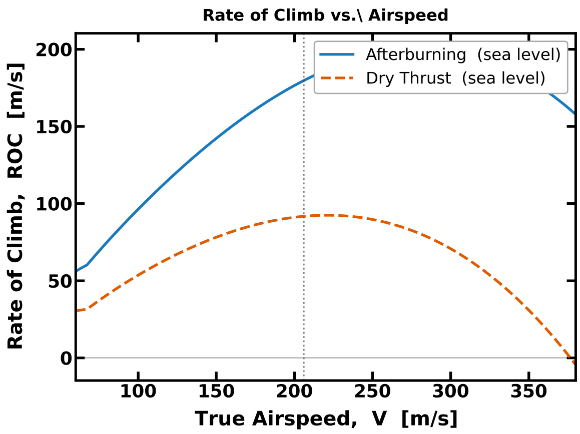

Figure 9: Rate of climb vs. airspeed.

Widely circulated open-source figures of 350–384 m/s would require approximately 274 kN or more per engine — roughly double the published AL-41F1 rating — and are therefore not derivable from any known variant of this engine (Butowski, 2022; McCormick, 1995).

5.8 Sensitivity and Propagated Uncertainty

Three principal input uncertainty groups are identified: (i) geometric inputs (S, AR, Λ_{LE}), nominally ±2–5%; (ii) drag-build inputs ($C_{D0} \in [0.015, 0.025]$, $e \in [0.85, 0.92]$ (Raymer, 2018; Traub, 2024)); (iii) propulsion data (±3% on quoted thrust). Linearised sensitivity of sustained turn rate to C_{D0} at the level-turn condition gives $\partial\omega/\partial C_{D0} \approx -68°/\text{s}$ per unit C_{D0}, so a ±0.005 uncertainty in C_{D0} alone yields ±0.34°/s. Combining the three groups in quadrature gives a one-sigma band of approximately $\pm 2.5^\circ$/s on sustained turn rate and ± 25 m/s on ROC. The 5–21% gap between the derived sustained turn rate and the lower end of cited values lies within this band; the $\sim 100\%$ gap in cited ROC does not.

6 Avionics and Electronic Warfare

The Su-57 incorporates the Sh121 integrated radar complex, comprising multiple AESA subsystems providing hemispheric situational awareness (Butowski, 2022; Wikipedia contributors, 2026a). Module counts and engagement capacities derive from Tikhomirov NIIP open-source disclosures aggregated by (Wikipedia contributors, 2026a) and have not been independently confirmed:

- **N036-1-01 Byelka (forward X-band)** — 1,514 T/R modules; simultaneous tracking of up to 60 targets, engagement of up to 16 (Wikipedia contributors, 2026a; Butowski, 2022).
- **N036B-1-01 (side-facing X-band)** — Two arrays, 404 T/R modules each, extending field-of-regard to $\pm 60^\circ$ beyond the forward sector (Wikipedia contributors, 2026a).
- **N036L-1-01 (L-band wing arrays)** — Leading-edge L-band arrays ($\lambda \approx 15$–30 cm) providing counter-stealth capability by exploiting resonance effects at which low-observable aircraft RCS is significantly elevated relative to X-band (Butowski, 2022; Zikidis et al., 2014).

The Sh121 operates in LPI modes using frequency agility and low-power waveforms, with data from all arrays fused with IRST, ELINT, and EW inputs (Butowski, 2022). The L402 Himalayas active jamming suite is housed in the tail cone and wing leading edges, providing passive emitter geolocation, active jamming, and ESM support (Butowski, 2022). The 101KS Atoll electro-optical system comprises the 101KS-V IRST with laser rangefinder and the 101KS-O Directed Infrared Countermeasures (DIRCM) system, believed to be the first operational DIRCM fitment on a fixed-wing fighter aircraft (Butowski, 2022; Aviationist, 2025).

7 Armament

The Su-57 carries all primary armament internally, preserving stealth across all mission profiles (Butowski, 2022; Aviationist, 2025). Four internal bays are provided: two main tandem bays (each $\approx$ 4.4 m $\times$ 0.9 m, total capacity four BVR missiles) and two side quick-launch bays (one short-range missile each, rapid-deploy mechanism demonstrated at Dubai Airshow 2025 (Aviationist, 2025)). Six external hardpoints are available but degrade the RCS profile (Butowski, 2022). An internal 30 mm GSh-30-1 cannon (150 rounds) is embedded in the right LEVCON root (Butowski, 2022).

Tables 3 and 4 summarise the air-to-air and air-to-ground loadouts respectively. The standard air-superiority stealth loadout is 4×R-77M in the main bays and 2×R-74M2 in the side bays.

Table 3: Su-57 air-to-air missile loadout (Butowski, 2022; Jane's Information Group, 2009; Zone, 2024)

Missile	**Guidance**	**Range**	**Role**
R-77M	Active radar	Medium-BVR	Primary BVR, main bays
R-74M2	Infrared	Short-range	WVR, side bays, 75° off-boresight
R-37M	Active radar	>300 km	Very long-range BVR

Table 4: Su-57 air-to-ground loadout (Butowski, 2022; Zone, 2024)

Weapon	**Range**	**Role**
Kh-69 (Kh-59MK2)	∼300 km	Precision strike, subsonic cruise missile
Kh-38M	Medium	Tactical air-to-ground
Kh-58UShK	>200 km	Anti-radiation SEAD, Mach 3.6
Kh-35U	Medium	Anti-ship
KAB-250L / KAB-500	—	Electro-optically/laser guided bombs

8 Operational Assessment

8.1 Strengths

- **Supermaneuverability** — LEVCON-TVC enables post-stall manouvering at $\alpha > 60°–70°$, independently validated by multiple peer-reviewed CFD and experimental studies (Malicki et al., 2023; Tsai et al., 2025; Burman et al., 2008; Atesoglu and Ozgoren, 2007; Francis, 2018). Provides a decisive WVR combat advantage.

- **Counter-stealth detection** — N036L L-band arrays partially offset the Su-57's own X-band stealth disadvantage by exploiting the elevated RCS of low-observable aircraft at longer wavelengths (Zikidis et al., 2014; Butowski, 2022).

- **Weapons breadth** — Internal carriage of BVR, WVR, SEAD, precision strike, and anti-ship munitions simultaneously with stealth preserved; R-37M provides >300 km BVR reach (Jane's Information Group, 2009).

- **Active self-defence** — 101KS-O DIRCM provides the first operational active IR countermeasure on a fixed-wing fighter (Butowski, 2022; Aviationist, 2025).

- **Supercruise confirmed** — Excess thrust margin of 68.1 kN at Mach 1.3 analytically verified in Section 5.

8.2 Limitations

- **Stealth inferiority** — Head-on X-band RCS of 0.1–1.0 m^2 substantially exceeds the F-22 ($< 10^{-4}\,m^2$) and F-35 ($\sim 10^{-3}\,m^2$); the absence of serpentine inlet ducts is the primary contributor (Zikidis et al., 2014).

- **Engine immaturity** — AL-41F1 is a derivative powerplant; the clean-sheet Izdeliye 30 (176 kN, 20% SFC improvement) had not entered production as of 2026 (The National Interest, 2025).

- **Low production rate** — Approximately 30 airframes delivered against a 76-aircraft contract as of early 2026, reflecting sanctions-driven avionics supply constraints (Defence, 2026; The National Interest, 2025).

- **Sensor fusion gap** — Sh121 complex reported to lag the F-35's integrated battlespace picture in multi-axis contested engagements (Butowski, 2022).
- **Limited operational record** — Ukraine-conflict deployments confined to standoff engagements; no large-scale operational use reported (The National Interest, 2025).

The Su-57 embodies a design philosophy that prioritises agility, sensor breadth, and cost over deep low-observable integration. In BVR engagements against Western fifth-generation fighters its higher RCS is a detectability liability; in WVR engagements its LEVCON-TVC architecture likely confers a decisive advantage (Malicki et al., 2023; Atesoglu and Ozgoren, 2007; Zikidis et al., 2014). The programme's primary constraint is industrial rather than technical: production rates remain insufficient to translate aerodynamic and systems performance into meaningful strategic mass (Defence, 2026; The National Interest, 2025).

9 Conclusion

This paper has presented an aerodynamic and systems-level analysis of the Sukhoi Su-57 applying USAF Digital DATCOM methodology (Williams and Vukelich, 1979) to publicly available geometric and propulsion data; no comparable peer-reviewed analysis has been identified in the open literature.

The principal derived aerodynamic results are:

- **Lift-curve slope:** $C_{L_\alpha} = 2.728\,\mathrm{rad}^{-1}$ (DATCOM, half-chord sweep 38°) (Williams and Vukelich, 1979)
- **Subsonic drag:** $D \approx 55.96\,\mathrm{kN}$ at sea level, $V = 206\,\mathrm{m/s}$ (Anderson, 2005; McCormick, 1995)
- **Supercruise excess thrust:** $T_{\mathrm{Excess}} \approx 68.1\,\mathrm{kN}$ at Mach 1.3, confirming AL-41F1 supercruise capability (Loftin, 1985)

- **Instantaneous turn rate:** $\dot{\psi} \approx 24.4°/\text{s}$, G-tolerance limited (McCormick, 1995; Hull, 2007)

- **Sustained turn rate:** $\dot{\psi} \approx 23.7°/\text{s}$ with full LEVCON and TVC augmentation (Malicki et al., 2023; Francis, 2018; Hull, 2007)

- **Rate of climb:** $ROC \approx 180.5\,\text{m/s}$ at $TWR = 1.09$, sea level (McCormick, 1995)

A consistent discrepancy is identified between derived and widely cited performance figures (Table 5). The sustained turn rate falls 5–21% below the lower bound of cited values, within the propagated uncertainty band. The widely circulated rate-of-climb figures of 350–384 m/s are shown to require approximately double the published AL-41F1 thrust and are not physically derivable from any known engine variant; these figures most likely correspond to unspecified low-weight zoom-climb conditions or originate from unverified secondary sources.

Table 5: Derived vs. cited performance figures (Butowski, 2022; McCormick, 1995; Hull, 2007)

Parameter	Derived	Cited	Discrepancy
Sustained Turn Rate	23.7°/s	25–30°/s	$\sim$ 5–21%
Rate of Climb	180.5 m/s	350–384 m/s	$\sim$ 94–113%

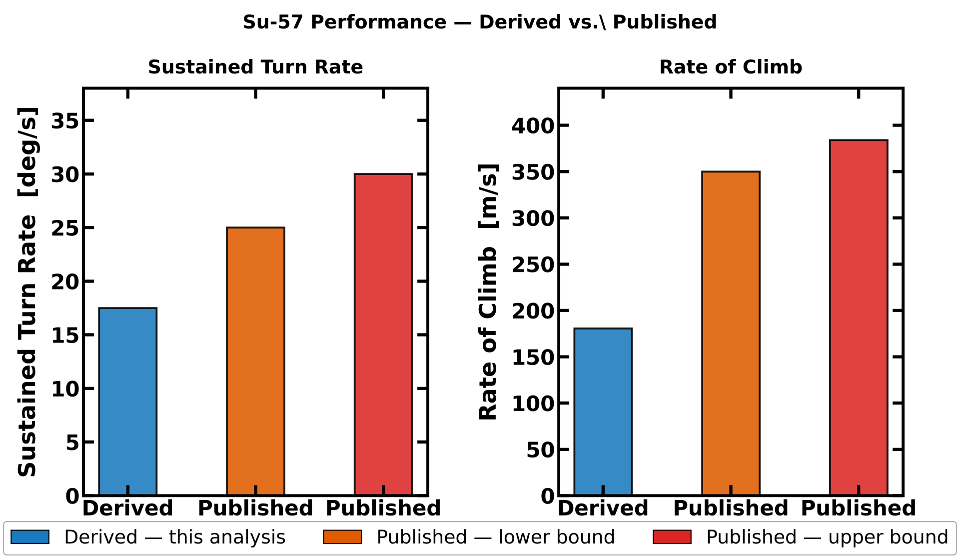

Figure 10: Derived vs. published performance (Butowski, 2022; McCormick, 1995).

The Su-57 represents a fifth-generation aerodynamic achievement: its LEVCON-TVC supermaneuverability architecture is unique among operational fifth-generation fighters and is independently validated by peer-reviewed studies (Malicki et al., 2023; Tsai et al., 2025; Burman et al., 2008; Atesoglu and Ozgoren, 2007); its N036L L-band arrays provide an innovative counter-stealth detection capability (Zikidis et al., 2014); and its internal weapons suite supports the full spectrum of air-superiority, SEAD, and strike missions with stealth preserved. The programme's primary constraint remains industrial — production rates are insufficient to translate these capabilities into strategic air power mass (Defence, 2026; The National Interest, 2025).

Known limitations and future work.

- LEVCON lift increment applied as a scalar from Malicki et al. Malicki et al. (2023); first-principles derivation requires LEVCON planform geometry not available in the public domain.
- Wave drag at supercruise treated as constant ($C_{D_{wave}} = 0.020$); a Mach-dependent transonic drag rise model (Kármán–Ogive or Lock approximation (Anderson, 2005)) will be incorporated in a future revision.
- All propulsion calculations assume sea-level static thrust scaled by published TWR; an altitude-dependent thrust-lapse model is planned (Raymer, 2018).
- DATCOM is conservative for blended wing-body configurations with LEVCON augmentation; vortex-lattice cross-validation using AVL or OpenVSP is planned (Williams and Vukelich, 1979).
- Calculations use AL-41F1 specifications; a performance comparison incorporating the Izdeliye 30 will be included when verified data become available (The National Interest, 2025).

All values are derived from publicly available data using USAF Digital DATCOM (Williams and Vukelich, 1979) and standard aerodynamic equations, and represent engineering approximations rather than definitive specifications.

Statements and Declarations

Declaration of conflicting interest. The author declared no potential conflicts of interest with respect to the research, authorship, and/or publication of this article.

Funding statement. The author received no financial support for the research, authorship, and/or publication of this article.

Data availability. All source data are drawn from publicly available open-source references cited herein. No proprietary or restricted data were used. Derived calculations are reproducible from the equations and input values stated in Section 5.

Author Contributions

A.S.: Conceptualisation, methodology, formal analysis, investigation, writing (original draft), writing (review and editing), visualisation.

Acknowledgments

The author acknowledges the USAF Digital DATCOM documentation (Williams and Vukelich, 1979) as the primary methodological reference for stability derivative derivations, and the open-access work of Malicki et al. Malicki et al. (2023) and Tsai et al. Tsai et al. (2025) for peer-reviewed LEVCON aerodynamic data.

References

Anderson JD (2005) *Fundamentals of Aerodynamics*. 4th edition. New York: McGraw-Hill.

Atesoglu O and Ozgoren MK (2007) High-alpha flight maneuverability enhancement of a fighter aircraft using thrust-vectoring control. *Journal of Guidance, Control, and Dynamics* 30(5): 1480–1493. DOI:10.2514/1.28620.

Aviationist T (2025) Russia shows off su-57's internal weapons bays for the first time. https://theaviationist.com/2025/11/11/russia-shows-off-su-57s-internal-weapons-bays/.

Burman A, Mohan S and Ramakrishna M (2008) Improvement of high alpha aerodynamics for compound delta wing aircraft using leading edge vortex controller. In: *46th AIAA Aerospace Sciences Meeting and Exhibit*. Reno, NV. DOI:10.2514/6.2008-336. AIAA Paper 2008-336.

Butowski P (2022) *Su-57 Felon*, *Modern Military Aircraft Series*, volume 2. Stamford, UK: Key Publishing.

Davydenko A (2013) Low-observable aircraft. Russian Federation Patent RU 2502643 C2.

Defence C (2026) Russia receives first su-57 delivery of 2026. https://www.calibredefence.co.uk/russia-receives-first-su-57-delivery-of-2026/.

Encyclopaedia Britannica (2024) Fifth-generation jet fighter. Encyclopaedia Britannica. https://www.britannica.com/technology/fifth-generation-jet-fighter.

Etkin B and Reid LD (1996) *Dynamics of Flight: Stability and Control*. 3rd edition. New York: Wiley.

Francis MS (2018) Air vehicle management with integrated thrust-vector control. *AIAA Journal* 56(12): 4741–4751. DOI:10.2514/1.J056768.

GlobalSecurityorg (2024a) Izdeliye-117 / AL-41F1 engine. GlobalSecurity.org Russia Military Programmes.https://www.globalsecurity.org/military/world/russia/izdeliye-117.htm.

GlobalSecurityorg (2024b) Radar cross section (RCS). https://www.globalsecurity.org/military/world/stealth-aircraft-rcs.htm.

Hull DG (2007) *Fundamentals of Airplane Flight Mechanics*. Berlin: Springer. DOI:10.1007/978-3-540-46573-7.

Jane's Information Group (2009) R-37, R-37M (AA-X-13), air-to-air missiles — beyond visual range. *Jane's Air-Launched Weapons* .

Kopp C and Goon PA (2010) Assessing the Sukhoi PAK-FA. Technical Report APA-2010-01, Air Power Australia. https://www.ausairpower.net/APA-2010-01.html.

Loftin LK (1985) *Quest for Performance: The Evolution of Modern Aircraft*. NASA SP-468. Washington, DC: NASA Scientific and Technical Information Branch. https://history.nasa.gov/SP-468/contents.htm.

Malicki L, Malecha Z and Tomczuk K (2023) Leading-edge vortex controller (LEVCON) influence on the aerodynamic characteristics of a modern fighter jet. *Energies* 16(22): 7590. DOI:10.3390/en16227590.

McCormick BW (1995) *Aerodynamics, Aeronautics, and Flight Mechanics*. 2nd edition. New York: Wiley.

Pillai RG (2019) Sizing of LEVCON surface for turn performance and controllability. In: *AIAA Aviation 2019 Forum*. Dallas, TX. DOI:10.2514/6.2019-2800. AIAA Paper 2019-2800.

Polhamus EC (1971) Predictions of vortex-lift characteristics by a leading-edge suction analogy. *Journal of Aircraft* 8(4): 193–199. DOI:10.2514/3.44254.

Raymer DP (2018) *Aircraft Design: A Conceptual Approach*. AIAA Education Series, 6th edition. Reston, VA: AIAA. DOI:10.2514/4.104909.

The National Interest (2025) Russia delivered few, if any, Su-57s in 2025. https://nationalinterest.org/blog/buzz/russia-delivered-few-if-any-su-57s-in-2025-ps-010926.

Traub LW (2024) Prediction of the oswald efficiency factor for cambered and swept wings. *Journal of Aircraft* 61(1): 317–322. DOI:10.2514/1.C037444.

Tsai YL, Chen WL and Hu MH (2025) A numerical study on the aerodynamic characteristics of leading-edge vortex controllers on a fighter pertinent to Su-57. *Aerospace Science and Technology* 166: 110610. DOI:10.1016/j.ast.2025.110610.

Wikipedia contributors (2026a) Byelka (radar). Wikipedia, The Free Encyclopedia. https://en.wikipedia.org/wiki/Byelka_(radar).

Wikipedia contributors (2026b) Sukhoi Su-57. Wikipedia, The Free Encyclopedia. https://en.wikipedia.org/wiki/Sukhoi_Su-57.

Williams JE and Vukelich SR (1979) The USAF stability and control digital DATCOM, volume I: Users manual. Technical Report AFFDL-TR-79-3032, Air Force Flight Dynamics Laboratory, Wright-Patterson AFB, OH. DTIC Accession No. ADA086557. Available: https://www.pdas.com/refs/AFFDL-TR-79-3032-Digdat-manual-DGS-scan.pdf.

Zikidis KC, Skondras A and Tokas C (2014) Low observable principles, stealth aircraft and anti-stealth technologies. *Journal of Computations & Modelling* 4(1): 129–165. http://www.scienpress.com/Upload/JCM/Vol%204_1_9.pdf.

Zone TW (2024) We finally get a clear look at the su-57 felon's side weapons bays. https://www.twz.com/air/we-finally-get-a-clear-look-at-the-su-57-felons-side-weapons-bays.